An experimental study on thermal runaway characteristics of lithium-ion batteries with high specific energy and prediction of heat release rate

Haodong Chen [a], Jonathan E.H. Buston [b], Jason Gill [b], Daniel Howard [b], Rhiannon C. E. Williams [b], Chandra M. Rao Vendra [a], Ashish Shelke [a], Jennifer X. Wen [a,*]

[a] *Warwick FIRE, School of Engineering, University of Warwick, Library Road, Coventry, CV4 7AL, UK*
[b] *The Health and Safety Executive Science and Research Centre, Harpur Hill, Buxton, SK17 9JN, UK*

HIGHLIGHTS

- Thermal runaway characteristics of type 21700 cylindrical cells are investigated.
- Characteristics of spark and jet fire during thermal runaway are analysed in detail.
- The effect of SOC on the battery fire behaviour is presented.
- Heat release rates of type 21700 battery fires are estimated using mean flame heights.

GRAPHICAL ABSTRACT

ARTICLE INFO

ABSTRACT

Understanding the potential thermal hazards of lithium-ion batteries (LIBs) during thermal runaway (TR) is helpful to assess the safety of LIB during storage, transport and use. This paper presents a comprehensive analysis of the thermal runaway (TR) characteristics of type 21700 cylindrical LIBs with a specific energy of 266 W·h/kg. The batteries with both 30% state of charge (SOC) and 100% SOC were triggered to TR by uniform heating using a flexible heater in a laboratory environment. Three high definition cameras and one high-speed camera were placed to capture TR behavior and flame evolution from different viewpoints. Correlation between the heat release rate (HRR) and the mean flame height of turbulent jet diffusion flame were used to estimate the HRRs of LIBs. Additional characteristics of cell failure (for cells with 100% and 30% SOC) were also noted for comparison, including: number of objects ejected from the cell; sparks and subsequent jet fires. An approach has been developed to estimate the HRRs from TR triggered fires and results compared with previous HRR measurements for type 18650 cylindrical cells with a similar cathode composition.

1. Introduction

The characterisation of lithium-ion battery (LIB) fires is becoming of increasing importance, not least to the rise in number of electric vehicles (EVs) being introduced over recent years. The vast majority of LIB fires can be traced back to LIB thermal runaway (TR) triggered by mechanical, electrical and/or thermal abuse [1–3], and incorporate complex chemical and physical processes, from decomposition of the electrode

---

materials and the burning of some of them, to the ejection of sparks and flammable gases as well as their combustion. During LIB thermal abuse tests, the thermal response of LIBs can be divided into three stages: a preheating stage, an exothermic stage, and a cooling stage. The transition process from LIB ignition to extinguishment occurs during the exothermic stage. Typical phenomena reported during LIB fires including sparks and jet fires were observed during TR in previous studies [4–17]. Sparks projected from LIBs were found to be capable of igniting vent gases generated within the LIB during TR [8]. Two jet fires were reported during single-cell LIB tests [4,6,13], with multiple jet fire events being observed in both single-cell LIB and LIB module tests [9,12, 18]. The maximum cell surface temperature and heat release rate (HRR) for different battery classifications and chemistries are summarized in Table 1. Maximum cell surface temperatures for fully charged, cylindrical, type 18650 LIBs have been reported in the range 311 to 876 °C. Measured flame temperatures as high as 1069 °C for single cells [8] and 1500 °C for a battery module [9] have been reported. In addition, there is evidence that observed mass loss rates decrease dramatically during evolution of the flame [4,6,8,9,12].

The HRR is an important parameter in evaluating the thermal hazards presented by LIB fires. The extent and duration of HRR influences TR propagation to neighbouring cells within a pack [14–16,19]. As shown in Table 1, the reported peak HRR for fully charged, cylindrical LIBs ranged between 1.1 kW and 11.8 kW. The distribution of the HRRs was found to only be weakly related to the nominal capacity of the LIBs under test. All HRRs reported in the literature [4–17,20] were calculated based on the oxygen consumption method [11], which is prone to both overestimation (due to the formation of carbon monoxide and soot particles [11,21]) and underestimation (due to oxygen release from the decomposition of the cathode materials [4,5]). Although these two effects offset each other to some extent, more accurate evaluation of the HRR of LIB fires using this method should quantitatively account for both them. Previous experimental work reported that, for a common LIB type, a higher state of charge (SOC) would lead to higher peak HRR [4,5, 9]. In addition, the chosen heating method [13] and incident heat flux [8,17] were found to have an influence on the observed HRR.

The effective range of EVs is being continuously improved through development of LIB technology providing higher energy densities. An example is type 21700 cylindrical cells (21 mm in diameter and 70 mm in height), which are adopted by Tesla Model 3 EVs due to their higher energy density and lower battery system cost than type 18650 cells [22]. Most previous studies of such commercial cylindrical LIBs have focused on the TR behaviour and HRRs of type 18650 cells. Although several

studies have been conducted to investigate the TR behaviour of LIBs, detailed analysis of type 21700 cell fire characteristics during TR is still lacking. Obtaining such insight can aid the development of mitigation measures and fire protection design of battery modules to enhance fire safety.

In this study, spark characteristics, the evolution from sparks to jet fire as well as the transition process of the jet fire produced by type 21700 cells during TR will be analysed. The effects of SOC on fire behaviour will also be investigated. Based on recorded transient mean flame heights of turbulent jet diffusion flame during type 21700 cell fires, HRRs of type 21700 battery fires have been estimated.

2. Experiments

The battery testing facility consists of three main sections: a ventilated burning chamber, a connected antechamber and a separate control room. All tests were performed within the burning chamber. Local exhaust ventilation (LEV) was switched on after cell ignition. The antechamber contains the data acquisition equipment and power supplies. The control room, from which staff can initiate and monitor the tests, is approximately 15 m away. Measurements were conducted for commercial type 21700 LIBs with lithium nickel manganese cobalt oxide (NMC) cathode. The nominal capacity and voltage of the cell type is 5 Ah and 3.63 V with the lower and upper voltage limits being 2.5 V and 4.2 V, respectively. The mass of the cell type is 68.3 ± 1.0 g with a specific energy as high as 266 W·h/kg. As shown in Fig. 1, the cell (with its plastic wrap removed) was secured by a clamp in the vertical position. It was heated to failure by an adhesive, 2" x 2" heating strip with resistance of 17.9 Ω (KHLVA-202/10-P, Omega). A heater voltage of 20 V was applied to the cell until failure was observed at which point the applied voltage was turned off. The voltage of the cell and temperature on the cell surface were measured by both a battery analyser (BST8-5A-CST, MTI) and a type K thermocouple respectively. The positioning of the heater and the thermocouple are shown in Fig. 1a. Data measured during tests were recorded by a data logger (GL840, Graphtec). Three high definition (HD) cameras (HD-SDI CCTV, NiteDevil) recording at 25 frames per second and one high-speed camera (Phantom Miro LC320s, AMETEK) recording at 1000 frames per second were used to capture footage of gaseous ejections during TR and the flame characteristics from different aspects. A schematic diagram showing camera positions is shown in Fig. 1b. One HD camera was positioned directly above the cell. The other HD cameras and the high-speed camera were each positioned at a stand-off distance of 1.5 m from the cell. The high-speed camera and

Table 1
Summary of experimental results in previous studies.

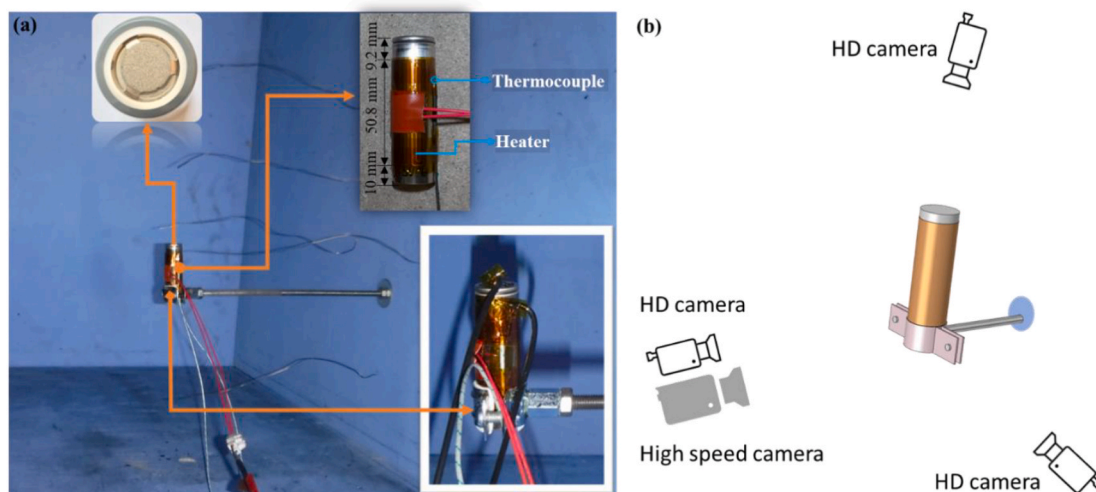| Classification	Cathode/anode materials	Nominal capacity (Ah)	Maximum temperature on cell surface (°C)	Peak heat release rate (kW)	Ref.
Cylindrical 18650 (18 mm in diameter and 65 mm in height)	Li(Ni$_x$Mn$_y$Co$_z$)O$_2$/carbon	2.25	454 ± 13	1.1	[7]
	Li(Ni$_x$Mn$_y$Co$_z$)O$_2$/graphite	3.2	703	1.3	[10]
	Li(Ni$_x$Mn$_y$Co$_z$)O$_2$/graphite	2.0	539 ± 23	3.75 ± 0.86	[14]
	Li(Ni$_{0.8}$Co$_{0.15}$Al$_{0.05}$)O$_2$/graphite	3.2	876	11.8 ± 0.05	[8]
	LiCoO$_2$/graphite	2.6	756 ± 56	4.1/3/3.3	[4]
	LiCoO$_2$/graphite	2.6	797	6.8	[5]
	LiCoO$_2$/carbon	2.6	428 ± 20	1.5	[7]
	LiFePO$_4$/graphite	1.3	621 ± 29	6.8/8.3/7	[4]
	LiFePO$_4$/carbon	1.5	311 ± 2	1.3	[7]
Pouch	LiMn$_2$O$_4$/graphite	2.9	Not given	21	[11]
Prismatic	Li(Ni$_x$Mn$_y$Co$_z$)O$_2$/graphite	50	665.4	37.08	[13]
	Li(Ni$_x$Mn$_y$Co$_z$)O$_2$/Li$_4$Ti$_5$O$_{12}$	50	405	40	[6]
	LiFePO$_4$/graphite	50	580	64.32	[12]
Module	LiFePO$_4$/graphite	50 (five cells in parallel)	645	49.4	[9]

Fig. 1. (a) The test apparatus and (b) a schematic diagram of camera positions.

one HD camera were set-up directly facing the cell, with the other recording a side-on view.

3. Results and discussion

Three tests with 100% SOC and three tests with 30% SOC under the same heating conditions were performed. As shown in Table 2, the first sharp rise in temperature for 100% SOC cells exhibited a rate of temperature rise greater than 15 °C/s; with their time of occurrence during the three tests at 927.4 s, 1038.8 s, and 1066.0 s, respectively. The duration of combustion was found to be greater than 10 s for 100% SOC cells, with the shortest time difference between the onset of temperature rise and ignition being 3.3 s, which is very short for any intervention to reduce cell temperature to prevent TR. The time to ignition of the 30% SOC cells was longer than for 100% SOC cells, with the combustion event also being shorter in duration. Cells with 100% SOC gives rise to a far more consistent temperature at the first sharp rise in temperature when compared to 30% SOC cells. An average of temperature at the first sharp rise in temperature of Tests 1–6 is 202.0 °C, which is probably a critical point at which a large amount of heat is generated by internal short circuit due to the separator melting.

3.1. Overall characteristics

Images from Test 1 are shown in Fig. 2 as a representative example of evolution from ignition to extinguishment for a 100% SOC cell. The initial stages of ignition are characterised by the ejecting of white smoke and gases. This was followed by production of sparks, a firework type effect, fireball, jet fire and extinguishment. On functioning of the cell pressure relief mechanism, white smoke and gases are released from the cell (Fig. 2a and b) and this is believed to consist mostly of carbon

Table 2
Summary of the experimental results.

SOC	Test sample	Time to ignition (s)	Duration of combustion (s)	Temperature at the first sharp rise in temperature (°C)	Maximum temperature on cell surface (°C)
100%	1	933.0	~15.2	187.6	583.5
	2	1048.5	~16.3	191.9	646.9
	3	1069.3	~11.1	189.7	707.3
30%	4	1398.3	~13.0	204.8	675.2
	5	1943.7	~15.7	189.5	727.7
	6	2757.5	~8.2	248.7	719.3

dioxide (CO_2) and electrolyte vapours [2,11,23–25]. At this point the concentration of any flammable vent gases is considered to be out with the flammability limits of the gas mixture, as no ignition by sparks has occurred. Venting continues in this manner until an initial burst of sparks is observed (Fig. 2c), which became increasingly bright. Spark production develops to produce a firework type effect which is clearly captured by the HD cameras. A fireball (Fig. 2d) was formed after the top cover of the cell was forced off by the ejecting sparks and gases. Subsequently, a jet fire occurred (Fig. 2e) until all combustible gases were consumed and the fire extinguished (Fig. 2f). Some soot was observed but there was no obvious swelling of the cell casing during TR. The production of white smoke and sparks has also been observed in large-scale LIB testing [13]. The behaviour of the sparks and the jet flame in Test 1 are now considered.

3.2. Sparks

Sparks are the first observed evidence of burning and occur before the cell fully catches fire. The sparks are small, incandescent particles of red, yellow, and silver/bright white colouration, being projected from the cell under high pressure generated by thermal decomposition events occurring within the cell. Initially, one relatively dull, red coloured spark was ejected from the cell. This was followed after a few milliseconds by a cluster of sparks, also red in colour bursting through a vent in the top cover of the cell. A further two clusters of sparks were observed to exit through the other two vents on the top cover as shown in Fig. S1 supplementary information. The colours of the sparks are determined, not only by their temperature (e.g. 'red hot' to 'white hot') but also by chemical composition. By cross-referencing the observed spark colours to those produced by specific elements (commonly used to produce firework colours [26]), it can be inferred that the observed sparks with red colouration are probably derived from lithium salts, including lithium carbonate (Li_2CO_3) produced by the decomposition and reaction of solid electrolyte interphase (SEI) material, ethylene carbonate (EC)-based electrolytes and the carbon-based anode [27] present within the cell. Silver/bright white sparks may be attributable to aluminium present in the aluminium current collector. No blue colouration was observed during the early stage of TR, it is inferred that no degradation of the copper current collector was taking place. From this it can be reasoned that the temperature inside the decomposing cell was between the melting point of aluminium (660.32 °C) and the melting point of copper (1084.62 °C) during this period [11]. The ejected sparks weakened gradually during the jet fire stage until they were no longer observable. The duration of the spark stage was less than 1.52 s.

Fig. 2. Evolution from ignition to extinguishment of the cell with 100% SOC captured by the HD camera: (a) white smoke and gases, (b) sparks, (c) firework, (d) fireball, (e) jet fire, and (f) extinguishment.

Fig. 3 shows the evolution of the sparks from a small number of jet spark events being projected in multiple directions into a larger cluster of vertically projected jet sparks. Although visually similar to a jet flame event, it was identified that during this stage of combustion, brilliant incandescence was caused by a dense concentration of sparks and not a true flame. It is assumed that these sparks are produced by combustion of the cathode material. The jet spark stage of the combustion event lasted 1.07 s. The next stage of combustion was development of jet sparks to a true jet flame, a transition that was captured by high-speed camera (Fig. 4). Large pieces of the carbon-based anode material alongside small pieces of copper current collector were observed to be ejected from the cell during the transition. After this transition process, there were few in number ejected from the cell. Several pieces of carbon-based anode material and copper foil ejected from the cell were observed falling to the ground and are shown in Fig. S2 (supplementary material). It is thought that jet sparks might have acted as ignition sources for the emitted gases, although it is also likely that some gases were already burning before being ejected from the cell. In summary, jet sparks were dominant at early stage and then a combination of the jet flame with jet sparks ejected from the cell, and finally the jet flame was dominating.

3.3. Jet fire

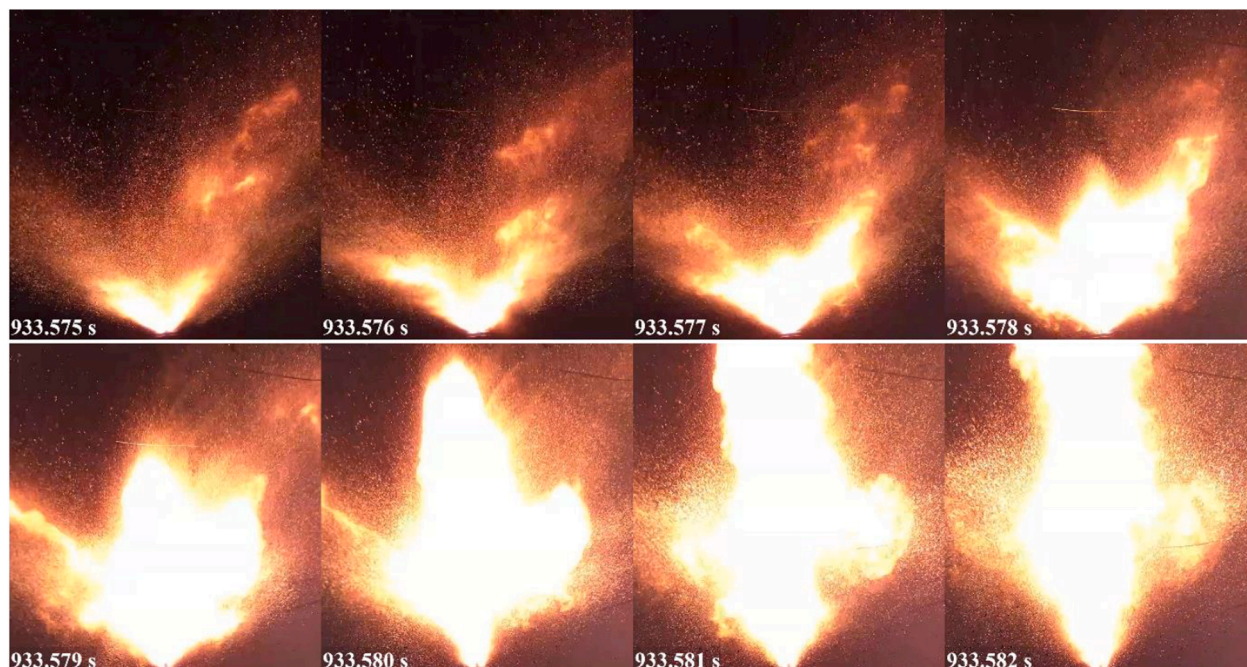The early stages of observed jet fire development are illustrated in Fig. 5. In general jet flames can be characterised based on their fire Froude number, which is less than 3 for buoyancy-controlled jet flame, and is greater than 5 for momentum-controlled jet flame, with any value in the range 3–5 indicating a transition between buoyancy and momentum [28]. In the case of the observed jet flame observed (Fig. 5), characterisation by fire Froude number is not possible as there are unknown parameters such as internal pressure during the event. However, general observations during the jet flame stage of combustion can be made. The flame spread almost monotonically upwards accompanied by sparks and pieces of the copper current collector. Items ejected from the test cell also have an influence on the flame shape, generally promoting its vertical spread. The flame colour and brightness were also found to change during this process. Fig. 6 illustrates the evolution of a torch-like jet fire, which is buoyancy-dominated in the upper part of the flame with some residual ejecting momentum in the lower parts. The buoyancy effect gradually becomes more dominant with the diminishing of momentum and the flame is observed to spread out in a radial direction with pulsing. It should be noted that the combustion of tape from the heater contributed to the fire during the latter stage of TR but the current tests could not separate these two. The phenomenon of flame lift-off has been reported for large-format LFP cells with 100% SOC [18], but was not observed during this study.

In order to further analyse the flame characteristics, the transient flame heights were evaluated by image processing using MATLAB®. The original images were extracted from the HD cameras and a threshold
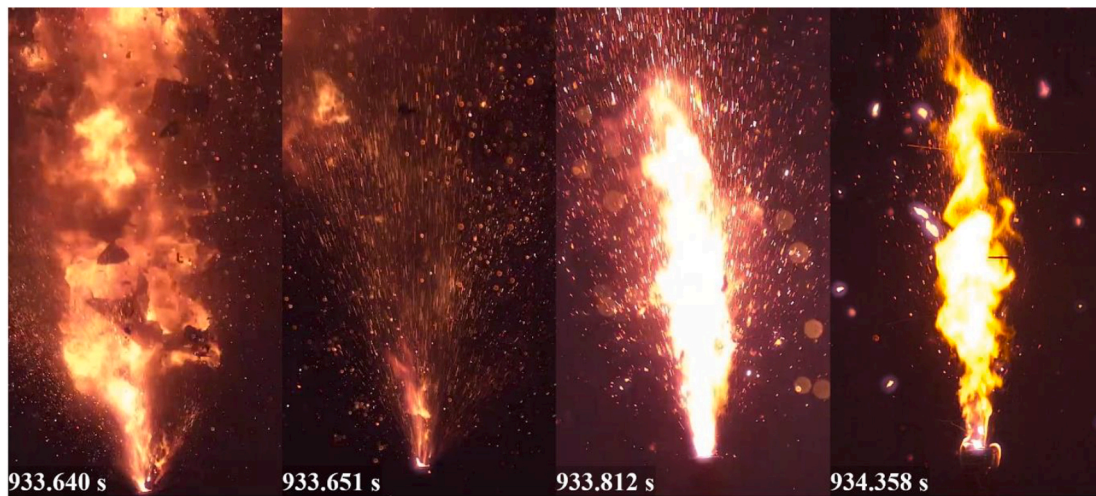

Fig. 3. Evolution of the cluster of jet sparks captured by the high-speed camera.

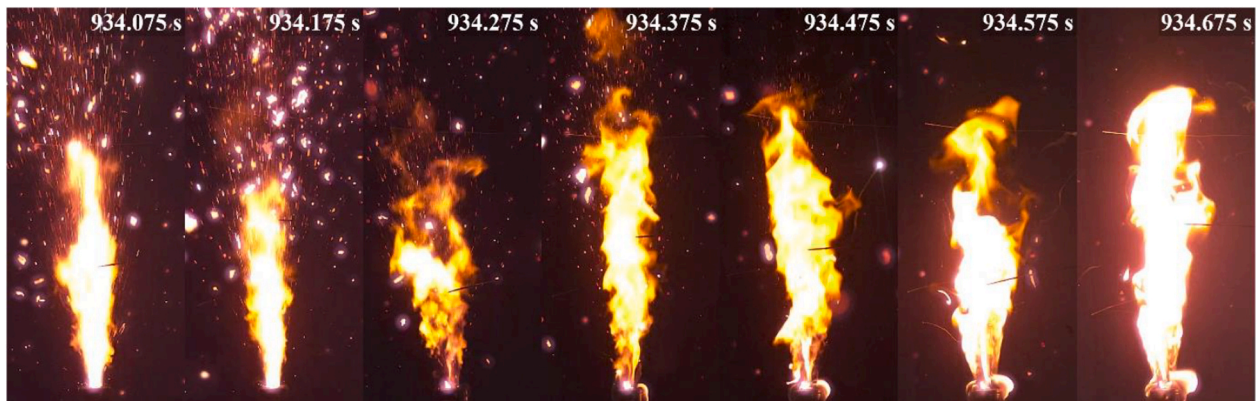**Fig. 4.** Evolution from sparks to jet fire captured by the high-speed camera.
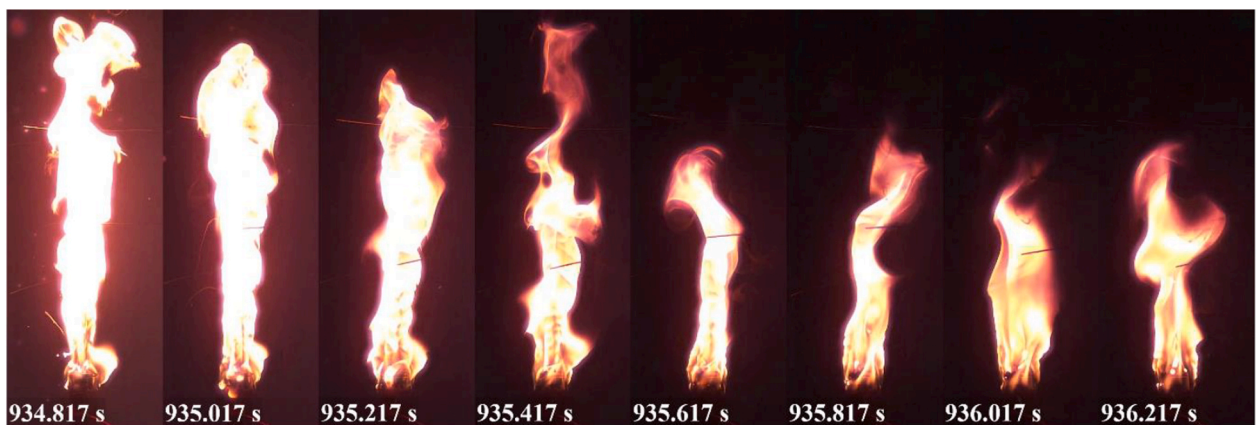

Fig. 5. Early stages of jet fire development.

Fig. 6. Evolution of the torch-like jet fire captured by the high-speed camera.

value of 0.9 set to obtain the corresponding binary images. It was not possible to use original images taken directly from the high-speed camera as in some frames flame heights exceeded the frame dimensions. The error between measured height and height calculated following image processing was found to be within 10% by directly comparing the flame heights recorded on the original image with those rendered on the corresponding binary image. Fig. 7a shows the obtained transient flame heights, which were observed to fluctuate due to a

combination of variations in ejection velocity, gas composition, available fuels and flame pulsating. A general downward trend in flame height is observed until the flame is extinguished. The maximum calculated flame heights were 318.5 $\pm$ 31.9 mm, 318.0 $\pm$ 31.8 mm and 333.3 $\pm$ 33.3 mm, respectively for the three tests. Start time ($t = 0$) in Fig. 7a is taken as the onset of ignition and flame heights were estimated after the formation of visible jet fire. During the latter stages of combustion there was some contribution from burning of the heater tape
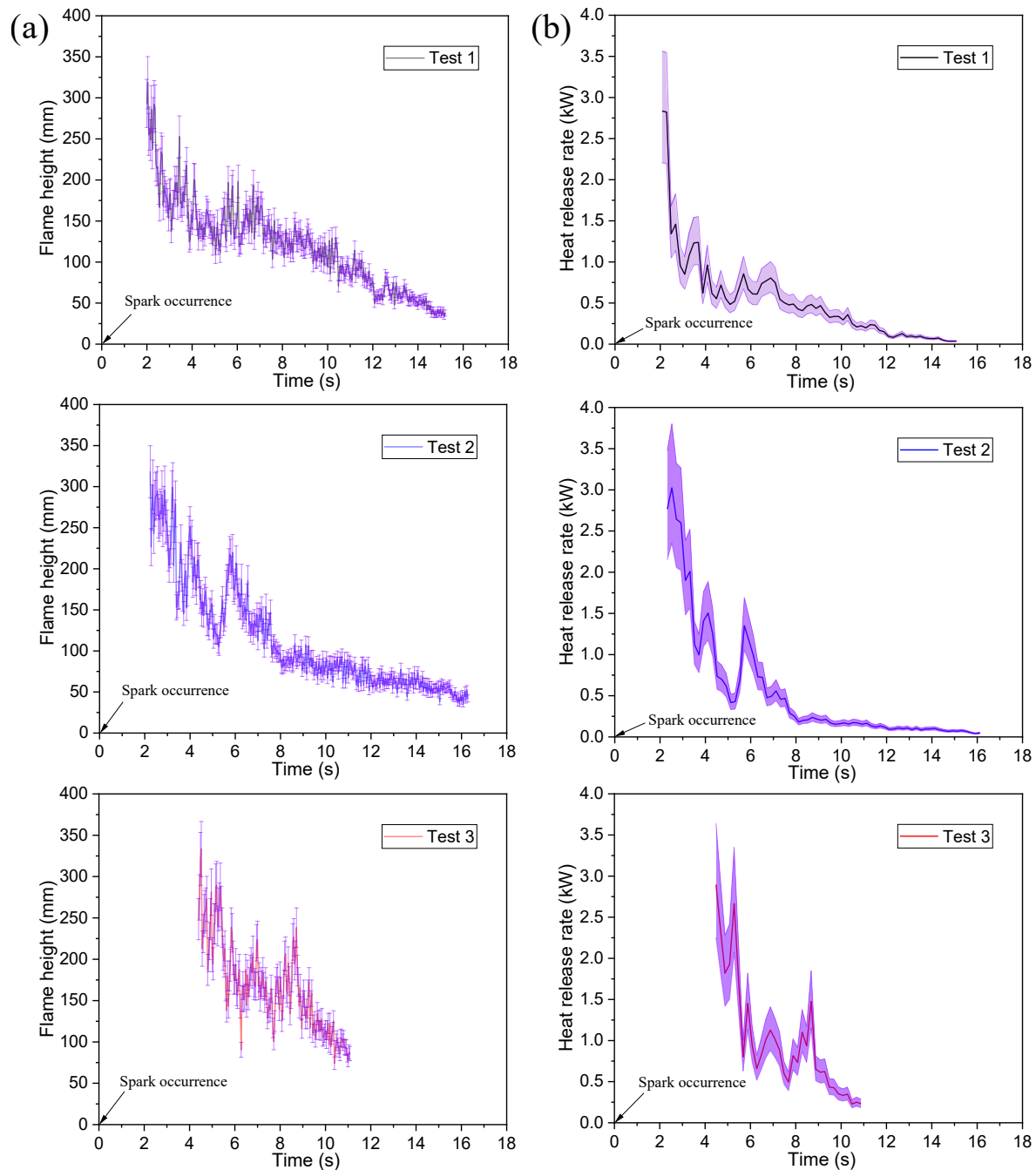
Fig. 7. (a) Flame height vs. time and (b) heat release rate vs. time for 100% SOC LIBs.

meaning the flame continued to burn, even after all the gaseous products had been ejected from the cell and consumed.

3.4. Effect of state of charge

Three tests with 30% SOC cells were conducted with the same heating condition as used for 100% SOC cells. During these tests, large quantities of smoke and gas were observed to vent from the cell prior to ignition. The sequence of events from point of ignition to extinguishment of 30% SOC cells are shown in Fig. 8. No violent jet fires were observed, which was significantly different from the tests for 100% SOC cells. As shown in Fig. 8a (Test 4), sparks were initially ejected from the cell, but the cell was not ignited. The cell used in Test 4 became bright red with an accompanying increase in temperature. After 5.92 s, the cell,

heater and heater tape ignited simultaneously and proceeded to burn until the fire extinguished. As shown in Fig. 8b–d (Tests 5 and 6), no sparks were observed prior to cell ignition. The cell, heater and heater tape in Tests 5 and 6 were ignited almost simultaneously. During the early stages of the jet fire, projection of flame in three directions was observed due to the top cover of the cell having three vents. The top cover of the cell was not blown away by the ejected gases, indicating a much less dynamic combustion process for 30% SOC cells when compared to the 100% SOC counterparts. As mentioned earlier, it is difficult to distinguish the relative contribution from the burning of the heater, heater tape and the cell to the overall energy generation. The duration of cell combustion was estimated by looking at flame shapes recorded over the duration of each test, with durations of 13.0 s, 15.7 s, and 8.2 s assigned for Tests 4, 5, and 6, respectively. For cells with 30%

Fig. 8. Evolution from ignition to extinguishment of the cell with 30% SOC captured by the HD camera.

SOC, the ejected flame was much weaker than that from the 100% SOC cells. The flame heights were not used to estimate heat release rate.

The fire behaviour of the 30% SOC cells was found to be less severe than their 100% SOC counterparts. An absence of jet fire had previously been reported for type 18650 LIBs with 50% SOC [14]. Since the ejected gas compositions have not been determined for type 21700 NMC cells, the fire behaviour at different SOCs can only be inferred from data obtained from other battery chemistries. On the one hand, as the SOC increased, the generated gas volume increased for LIBs with $LiCoO_2$ (LCO), $LiFePO_4$ (LFP) and $Li(Ni_{0.8}Co_{0.15}Al_{0.05})O_2$ (NCA) cathodes [23, 29–31] and the number of gas compositions also increased [32]. Such results indicate that chemical reactions occurring inside the cell become more violent for higher SOC. On the other hand, the amount of CO_2 within the ejected gas streams has been shown to decrease with increasing SOC [24] indicating that vent gas mixtures produced by higher SOC cells have a wider flammability range [23,24,31] and are more easily ignited. Using the findings of this current study, it can be inferred that the amount of CO_2 generated at 30% SOC is greater than that generated at 100% SOC. That the ejected gases were not ignited can be attributed to the concentration of the gas mixture falling below its lower flammability limit. The short duration of cell combustion observed in Tests 4–6 (Fig. 8) being related to the presence of smaller quantities of flammable gas mixture being present within its flammability limits.

4. Prediction of heat release rate

Heskestad [33] has proposed the following relationships between the heat release rate of flame ($\dot{Q}$) and the mean flame height for vertical turbulent jet flames (L_f).

$$\frac{L_f}{L_B} = \begin{cases} 1.2 & R_M < 0.1 \\ 0.405 R_M^{-1/2} & R_M \geq 0.1 \end{cases} \tag{1}$$

where L_B is the purely buoyancy-controlled flame height and R_M is a ratio of gas release momentum to the momentum generated by a purely buoyant diffusion flame. They can be calculated as follows:

$$L_B / D = -1.02 + 15.6 N^{1/5} \tag{2}$$

$$R_M = 1.36 \left[\left(\frac{T_\infty}{T_f} \right) \left(\frac{c_P \Delta T_f}{(H_c/r)} \right)^{4/5} \right] \left(\frac{\rho_\infty/\rho_s}{r^2} \right) N^{2/5} \tag{3}$$

where N is a non-dimensional parameter and ρ_s is the density of the ejected gases in the discharge stream written by:

$$N = \left[\frac{c_P T_\infty}{g \rho_\infty^2 (H_c/r)^3} \right] \frac{\dot{Q}^2}{D^5} \tag{4}$$

$$\rho_s = \left(1 + \frac{\kappa - 1}{2} M^2 \right)^{-\frac{1}{\kappa-1}} \frac{P_s}{P_\infty} \frac{T_\infty}{T_s} \rho_{s\infty} \tag{5}$$

where T_∞ is the ambient temperature, ρ_∞ the ambient density, $\rho_{s\infty}$ the density of ejected gases at ambient temperature and pressure, C_P the specific heat of air at constant pressure, T_f the plume centreline temperature at mean flame height, ΔT_f the temperature difference between T_f and T_∞, H_c the actual lower heat of combustion of the mixed gases, r the actual mass stoichiometric ratio of air to the mixed combustible gases, P_s the internal pressure of the cell, T_s the internal temperature of the cell, g the standard acceleration due to gravity, and D the diameter of venting. The Mach number can be calculated from the following equation [34].

$$M = \begin{cases} \sqrt{\frac{2}{\kappa - 1} \left[\left(\frac{P_s}{P_\infty} \right)^{\frac{\kappa-1}{\kappa}} - 1 \right]}, \frac{P_\infty}{P_s} > \left(\frac{2}{\kappa+1} \right)^{\frac{\kappa}{\kappa-1}}, \text{ subsonic flow} \\ 1, \qquad\qquad \frac{P_\infty}{P_s} \leq \left(\frac{2}{\kappa+1} \right)^{\frac{\kappa}{\kappa-1}}, \text{ choked flow} \end{cases} \tag{6}$$

In order to compute the heat release rate, the composition of the ejected gases needs to be known. Baird et al. [24] have recently reviewed the ejected gas composition during TR in LIB cells. The gases mainly consist of hydrogen, carbon monoxide, hydrocarbons, and carbon dioxide. To the authors' knowledge, there are only two references that have measured the vent gas composition of cylindrical NMC cells. One was conducted by Golubkov et al. [35] for single type 18650 NMC cell during TR with the other conducted by Said et al. [19] for type 18650 NMC cell arrays during TR propagation. Due to the limited information available on the venting gases of NMC cells during the TR, the composition of the total collected ejected gases were estimated from the tests of Golubkov et al. [35] for a single cell with a similar cathode type, and were expressed as molar fractions:30.8% for H_2; 41.2% for CO_2; 13.0% for CO; 6.8% for CH_4 and 8.2% for C_2H_4. The estimated specific heat ratio of the gas mixture (κ) is 1.38 (CO_2 is excluded as it does not participate in combustion), which is calculated by $\kappa = 1 + 1/\Sigma(x_i/(\kappa_i - 1))$, where x_i and κ_i are the mole fraction and the specific heat ratio of each gas of gas mixture. The internal pressures within the cell were observed to change over time during TR. Values were as high as 16 bar [36] and 12.5 bar [37] have been reported prior to venting for type 18650 LIBs, with pressures decreasing dramatically after breaking of the vent cap. It dropped to 5.3 bar when the temperature on cell surface reached 300 °C [37]. The burst pressures of MTI (Material Technology International

Corporation) and LG type 18650 LIBs have been reported, with mean values of 2.158 MPa and 1.906 MPa, and peak values of 2.364 MPa and 1.961 MPa respectively [38].

In our own studies, no convenient means of measuring internal pressure in cylindrical LIBs during TR has been found so far. Given this limited information on the internal pressure, we have chosen to assume the internal pressure is greater than atmospheric pressure but not greater than 2.364 MPa. The parameters used in order to estimate the HRR are listed in Table 3.

The calculated maximum of R_M is 0.04, which is less than 0.1 for an HRR which is around four times peak measured value of 18650 NMC cells in Table 1. The R_M is still less than 0.1 when the H_c changes with 30%. It indicates that the mean flame height of turbulent jet flames of the cell is proportional to the purely buoyancy-controlled flame height even if mole fraction of ejected mixed gas or gas composition change slightly. A time averaged flame height is adopted here to represent the mean flame height with 50% flame intermittency since the internal pressure has been changing. In this study, the average flame height of every five frames is used to replace the mean flame height. This processing method will slightly exaggerate the mean flame height due to the limit of frame numbers.

Fig. 7b presents the estimated HRR with time for 100% SOC cells. The estimated peak HRRs for tests 1, 2 and 3 are 2.88 ± 0.68 kW, 3.08 ± 0.73 kW, and 2.95 ± 0.69 kW, respectively. These estimates are larger than the previously reported peak HRRs of 1.1 kW [7] and 1.3 kW [10], but less than the value of 3.75 ± 0.86 kW [14] for 18650 LIBs with a similar cathode. The HRR depends on many parameters as shown in the above equations. The ejected gas composition and internal pressure during TR are vital to accurately calculate HRRs. In addition, note that the correlations of Heskestad [33] were developed and validated for jet fires with fuel gas being initially at typical environment temperature. The elevated temperature of the released gases inside the cell was considered during the computation for the density of the released gas mixtures. The validity of the correlations will be further investigated when more parameters such as measured HRRs and ejected gas composition are available.

5. Conclusions

The high specific energy type 21700 LIBs with different SOCs under uniform electrical heating were conducted. The whole process from venting to TR, and the resulting fire were recorded by HD and high-speed cameras. The characteristics of spark and jet fire events during the combustion of cells were analysed. The transient flame heights were calculated by image processing. The effects of SOC on fire behaviour were presented and explained with flammability limit analysis and vent gas components of type 18650 LIBs. Published correlations between HRR and the mean flame height of turbulent jet diffusion flames were extended to estimate the HRRs in the cell fire. HRR predictions were compared with the reported values for similar LIB cells. The main

Table 3
Parameters used for calculating the HRR.

Parameter	Value	Unit	Source
C_p	1000	J/kg/K	
D	0.01	m	Measured
g	9.81	m/s^2	
H_C	6.25E+07	J/kg	Calculated
P_s	(1.01E+05, 23.64E+05]	Pa	Estimated
P_∞	1.01E+05	Pa	
r	10.8		Calculated
T_s	1023	K	Estimated
T_∞	293	K	Estimated
ΔT_f	500	K	[33]
κ	1.38		Calculated
$\rho_{s\infty}$	0.524	kg/m^3	Calculated
ρ_∞	1.20	kg/m^3	

conclusions are as follows:

(1) Many pieces of carbon-based anode material and copper foil were ejected from the cell with 100% SOC during the transition from jet sparks to fire.

(2) The fire behaviour of the cell with 30% SOC was less severe than that with 100% SOC for type 21700 LIBs. The reasons for more severe fire behaviour for cells with higher SOC are thought to be due to an increase in the number and rate of chemical reactions taking place inside the cell during TR, resulting in more combustible gases being ejected, and this ejected gas mixture having a wider flammability limit range.

(3) No direct measurements for the ejected gas composition or internal pressure during TR of type 21700 NMC cells with high energy density were made. The total collected gases were adopted to estimate the lower heat of combustion of the mixed combustible gases. The varying internal pressure possibly covering the pressure generated by chemical reactions inside the cell were used to calculate the ratio of ejected gas release momentum to the momentum generated by a purely buoyant diffusion flame. The estimated HRRs were in line with that reported for 18650 LIBs with similar cathode, illustrating the feasibility of calculating the HRRs by the flame heights of LIB fire using the correlations proposed by Heskestad [33].

The present approach can be used as an alternative means to estimate the HRRs in addition to the commonly used oxygen consumption method which also has its limitations. The correlations will be further modified when the measured HRRs, the ejected gas composition and the internal pressure are available.

Declaration of competing interest

The authors declare that they have no known competing financial interests or personal relationships that could have appeared to influence the work reported in this paper.

CRediT authorship contribution statement

Haodong Chen: Conceptualization, Methodology, Software, Visualization, Writing - original draft, Writing - review & editing. **Jonathan E.H. Buston:** Resources, Investigation, Methodology, Writing - review & editing. **Jason Gill:** Resources, Investigation, Methodology, Writing - review & editing. **Daniel Howard:** Investigation, Validation. **Rhiannon C.E. Williams:** Investigation, Validation. **Chandra M. Rao Vendra:** Writing - review & editing. **Ashish Shelke:** Writing - review & editing. **Jennifer X. Wen:** Conceptualization, Methodology, Supervision, Writing - review & editing.

Appendix A. Supplementary data

Supplementary data to this article can be found online at https://doi.org/10.1016/j.jpowsour.2020.228585.

References

[1] Q. Wang, P. Ping, X. Zhao, G. Chu, J. Sun, C. Chen, Thermal runaway caused fire and explosion of lithium ion battery, J. Power Sources 208 (2012) 210–224.

[2] X. Feng, M. Ouyang, X. Liu, L. Lu, Y. Xia, X. He, Thermal runaway mechanism of lithium ion battery for electric vehicles: a review, Energy Storage Mater. 10 (2018) 246–267.

[3] Q. Wang, B. Mao, S.I. Stoliarov, J. Sun, A review of lithium ion battery failure mechanisms and fire prevention strategies, Prog. Energy Combust. Sci. 73 (2019) 95–131.

[4] M. Chen, D. Zhou, X. Chen, W. Zhang, J. Liu, R. Yuen, J. Wang, Investigation on the thermal hazards of 18650 lithium ion batteries by fire calorimeter, J. Therm. Anal. Calorim. 122 (2015) 755–763.

[5] Y. Fu, S. Lu, K. Li, C. Liu, X. Cheng, H. Zhang, An experimental study on burning behaviors of 18650 lithium ion batteries using a cone calorimeter, J. Power Sources 273 (2015) 216–222.

[6] P. Huang, Q. Wang, K. Li, P. Ping, J. Sun, The combustion behavior of large scale lithium titanate battery, Sci. Rep. 5 (2015) 7788.

[7] X. Liu, Z. Wu, S.I. Stoliarov, M. Denlinger, A. Masias, K. Snyder, Heat release during thermally-induced failure of a lithium ion battery: impact of cathode composition, Fire Saf. J. 85 (2016) 10–22.

[8] P. Ping, D. Kong, J. Zhang, R. Wen, J. Wen, Characterization of behaviour and hazards of fire and deflagration for high-energy Li-ion cells by over-heating, J. Power Sources 398 (2018) 55–66.

[9] P. Ping, Q. Wang, P. Huang, K. Li, J. Sun, D. Kong, C. Chen, Study of the fire behavior of high-energy lithium-ion batteries with full-scale burning test, J. Power Sources 285 (2015) 80–89.

[10] J.G. Quintiere, Measuring the energetics of a lithium ion battery in thermal runaway, in: A. Snegirev, N.A. Liu, F. Tamanini, D. Bradley, V. Molkov, N. Chaumeix (Eds.), Proceedings of the Ninth International Seminar on Fire and Explosion Hazards (ISFEH9), Saint-Petersburg Polytechnic University Press, 2019, pp. 870–880.

[11] P. Ribière, S. Grugeon, M. Morcrette, S. Boyanov, S. Laruelle, G. Marlair, Investigation on the fire-induced hazards of Li-ion battery cells by fire calorimetry, Energ. Environ. Sci. 5 (2012) 5271–5280.

[12] Q. Wang, P. Huang, P. Ping, Y. Du, K. Li, J. Sun, Combustion behavior of lithium iron phosphate battery induced by external heat radiation, J. Loss. Prevent. Proc. 49 (2017) 961–969.

[13] Z. Wang, H. Yang, Y. Li, G. Wang, J. Wang, Thermal runaway and fire behaviors of large-scale lithium ion batteries with different heating methods, J. Hazard Mater. 379 (2019) 120730.

[14] G. Zhong, B. Mao, C. Wang, L. Jiang, K. Xu, J. Sun, Q. Wang, Thermal runaway and fire behavior investigation of lithium ion batteries using modified cone calorimeter, J. Therm. Anal. Calorim. 135 (2019) 2879–2889.

[15] M. Chen, O. Dongxu, S. Cao, J. Liu, Z. Wang, J. Wang, Effects of heat treatment and SOC on fire behaviors of lithium-ion batteries pack, J. Therm. Anal. Calorim. 136 (2019) 2429–2437.

[16] D. Ouyang, M. Chen, J. Wang, Fire behaviors study on 18650 batteries pack using a cone-calorimeter, J. Therm. Anal. Calorim. 136 (2019) 2281–2294.

[17] Z. Wang, D. Ouyang, M. Chen, X. Wang, Z. Zhang, J. Wang, Fire behavior of lithium-ion battery with different states of charge induced by high incident heat fluxes, J. Therm. Anal. Calorim. 136 (2019) 2239–2247.

[18] S. Wang, Z. Du, Z. Han, Z. Zhang, L. Liu, J. Hao, Study of the temperature and flame characteristics of two capacity LiFePO4 batteries in thermal runaway, J. Electrochem. Soc. 165 (2018) A3828–A3836.

[19] A.O. Said, C. Lee, S.I. Stoliarov, Experimental investigation of cascading failure in 18650 lithium ion cell arrays: impact of cathode chemistry, J. Power Sources 446 (2020) 227347.

[20] A. Lecocq, G.G. Eshetu, S. Grugeon, N. Martin, S. Laruelle, G. Marlair, Scenario-based prediction of Li-ion batteries fire-induced toxicity, J. Power Sources 316 (2016) 197–206.

[21] G.G. Eshetu, S. Grugeon, S. Laruelle, S. Boyanov, A. Lecocq, J.-P. Bertrand, G. Marlair, In-depth safety-focused analysis of solvents used in electrolytes for large scale lithium ion batteries, Phys. Chem. Chem. Phys. 15 (2013) 9145–9155.

[22] J.B. Quinn, T. Waldmann, K. Richter, M. Kasper, M. Wohlfahrt-Mehrens, Energy density of cylindrical Li-ion cells: a comparison of commercial 18650 to the 21700 cells, J. Electrochem. Soc. 165 (2018) A3284–A3291.

[23] T. Maloney, Lithium Battery Thermal Runaway Vent Gas Analysis, US Department of Transportation, 2016.

[24] A.R. Baird, E.J. Archibald, K.C. Marr, O.A. Ezekoye, Explosion hazards from lithium-ion battery vent gas, J. Power Sources 446 (2020) 227257.

[25] U. Bergström, Å. Gustafsson, L. Hägglund, C. Lejon, D. Sturk, T. Tengel, Vented Gases and Aerosol of Automotive Li-Ion LFP and NMC Batteries in Humidified Nitrogen under Thermal Load, Försvarets Forskningsinstitut FOI, 2015.

[26] B.J. Kosanke, K.L. Kosanke, C. Jennings-White, Pyrotechnic spark generation, in: Proceedings of the 3rd International Symposium on Fireworks, Lake Buena Vista, Florida, U.S.A., 1996, p. 233.

[27] P. Verma, P. Maire, P. Novák, A review of the features and analyses of the solid electrolyte interphase in Li-ion batteries, Electrochim. Acta 55 (2010) 6332–6341.

[28] M.A. Delichatsios, Transition from momentum to buoyancy-controlled turbulent jet diffusion flames and flame height relationships, Combust. Flame 92 (1993) 349–364.

[29] V. Somandepalli, K. Marr, Q. Horn, Quantification of combustion hazards of thermal runaway failures in lithium-ion batteries, SAE Int. J. Altern. Powertrains 3 (2014) 98–104.

[30] A.W. Golubkov, S. Scheikl, R. Planteu, G. Voitic, H. Wiltsche, C. Stangl, G. Fauler, A. Thaler, V. Hacker, Thermal runaway of commercial 18650 Li-ion batteries with LFP and NCA cathodes–impact of state of charge and overcharge, RSC Adv. 5 (2015) 57171–57186.

[31] W. Li, H. Wang, Y. Zhang, M. Ouyang, Flammability characteristics of the battery vent gas: a case of NCA and LFP lithium-ion batteries during external heating abuse, J. Energy Storage 24 (2019) 100775.

[32] Z. Liao, S. Zhang, K. Li, M. Zhao, Z. Qiu, D. Han, G. Zhang, T.G. Habetler, Hazard analysis of thermally abused lithium-ion batteries at different state of charges, J. Energy Storage 27 (2020) 101065.

[33] G. Heskestad, Turbulent jet diffusion flames: consolidation of flame height data, Combust. Flame 118 (1999) 51–60.

[34] P.T. Coman, S. Mátéfi-Tempfli, C.T. Veje, R.E. White, Modeling vaporization, gas generation and venting in Li-ion battery cells with a dimethyl carbonate electrolyte, J. Electrochem. Soc. 164 (2017) A1858–A1865.

[35] A.W. Golubkov, D. Fuchs, J. Wagner, H. Wiltsche, C. Stangl, G. Fauler, G. Voitic, A. Thaler, V. Hacker, Thermal-runaway experiments on consumer Li-ion batteries with metal-oxide and olivin-type cathodes, RSC Adv. 4 (2014) 3633–3642.

[36] M. Ottaway, Stability of Li-ion batteries; internal pressure measurement. http://www.inforlab-chimie.fr/doc/document_fichier_284.pdf.

[37] B. Lei, W. Zhao, C. Ziebert, N. Uhlmann, M. Rohde, H. Seifert, Experimental analysis of thermal runaway in 18650 cylindrical Li-ion cells using an accelerating rate calorimeter, Batteries 3 (2017) 14.

[38] F.A. Mier, Measurement of 18650 Format Lithium Ion Battery Vent Mechanism Flow Parameters, New Mexico Institute of Mining and Technology, 2018.